The effects of Stefan flow on the flow surrounding two closely spaced particles

Thamali R. Jayawickrama [a,*], M.A. Chishty [a], Nils Erland L. Haugen [a,b], Matthaus U. Babler [c], Kentaro Umeki [a,*]

[a] *Energy Engineering, Div. Energy Science, Luleå, University of Technology, 971 87 Luleå, Sweden*
[b] *Department of Thermal Energy, SINTEF Energy Research, Kolbjørn Hejes vei 1 A, 7491 Trondheim, Norway*
[c] *Department of Chemical Engineering, KTH Royal Institute of Technology, SE-10044 Stockholm, Sweden*

A R T I C L E   I N F O

A B S T R A C T

The aim of the work was to study the effects of neighboring particles with uniform Stefan flow in particle–fluid flows. Particle-resolved numerical simulations were carried out for particles emitting a uniform Stefan flow into the bulk fluid. The bulk fluid was uniform and isothermal. The Stefan flow volume emitted from the two particles is equal, such that it represents idealized conditions of reacting particles. Particles were located in tandem arrangement and particle distances were varied between 1.1 and 10 particle diameters ($1.1 \leq L/D \leq 10$). Three particle Reynolds numbers were considered during the simulations ($Re = 2.3, 7$ and 14), which is similar to our previous studies. Three Stefan flow velocities were also considered during simulations to represent inward, outward, and no Stefan flow. The drag coefficient of the particles without Stefan flow showed that the results fit with previous studies on neighbor particle effects. When the particle distance is greater than 2.5 diameters ($L/D > 2.5$), the effects of Stefan flow and neighboring particles are independent of each other. I.e. an outward Stefan flow decreases the drag coefficient (C_D) while an inward Stefan flow increases it and the *upstream* particle experience a higher C_D than the *downstream* particle. When $L/D \leq 2.5$, the effect of Stefan flow is dominant, such that equal and opposite pressure forces act on the particles, resulting in a repelling force between the two neighboring particles. The pressure force showed a large increase compared to the viscous force at these distances. The effect of Stefan flow is weakened at higher Reynolds numbers. A model was developed for the calculation of the drag coefficient. The model, which reproduce the results from the numerical simulations presented above, is a product of independent models that describe the effects of both neighboring particles and two distinguished effects of the Stefan flow.

1. Introduction

For an isolated particle in a highly dilute flow, accurate expressions for heat, mass and momentum transfer between particle and fluid are well known. This is not, however, the case for particle neighbors, which indirectly influence each other over a distance of several particle diameters through their exchange of heat, mass, and momentum with the fluid. As a result, the heat, mass, and momentum transfer between the fluid and a given particle may be significantly modified due to the presence of another particle in its vicinity. Understanding the physics behind these effects is therefore important for applications such as droplet evaporation, particle drying, and pulverized fuel combustion/gasification.

Droplet evaporation and combustion are complex phenomena involving various interactions such as reaction/phase change, changes to thermophysical properties, droplet break-up and collisions, particle–fluid interactions, and many more. A lot of scientific effort based on numerical simulations in droplet evaporation and combustion has exerted more towards creating more realistic conditions, especially chemical reactions in arrays of particles (Wang et al., 2020; Kékesi et al., 2019; Dwyer et al., 2000; Raju and Sirignano, 1990; Sirignano, 1993). Work related to droplet evaporation is not discussed here, and recent developments can be found in Kékesi et al. (2019) and Stefanitsis et al. (2019). There are some work also on coal/char combustion simulations with multiple neighboring particles (See for example Sayadi et al. (2017)). Sayadi et al. (2017) have investigated the effects of the position of a particle in an array on the char combustion behavior. They have found that particles facing the incoming flow have the highest burning rate and that the burning rate drops in consecutive particle

---

* Corresponding authors.

E-mail addresses: thamalirajika@gmail.com (T.R. Jayawickrama), kentaro.umeki@ltu.se (K. Umeki).

rows. This effect is stronger when the distance between rows is less than three particle diameters. However, these studies do not provide the fundamental information that is necessary to explain the phenomena causing these effects.

Interactions among particles play a crucial role in non-diluted particle–fluid flows. Particle flows can be categorized into isolated particles, particle arrays, particle streams, and particle clouds (Annamalai and Ryan, 1992). In the case of very dilute particle concentrations, a particle can be considered isolated. Interactions between a bulk fluid and an isolated particle immersed in it are well studied. However, it is clear that individual particles cannot be approximated as isolated in many practical applications, such as e.g. packed and fluidized beds. Furthermore, it is also true that even in significantly more dilute flows, as can be found, for example, in entrained flow gasifiers or pulverized burners, where particle volume fractions are very low (10^{-2}–10^{-4}) and particle separation distances are high ($L/D \approx 10$) (Göktepe et al., 2016b; García Llamas et al., 2020), the isolated particle approximation fails. Particle interactions can be categorized into two categories, where particle–particle interactions are direct collisions between particles, while particle–fluid–particle interactions are interactions where the fluid transmits the effect of one particle to another particle (such as the effect of the boundary layer of one particle on a neighboring particle's boundary layer). Particle–fluid–particle interactions are important in arrays, clouds and streams of particles. Much work has been done related to particle interactions in structured arrays and particle clouds (Yali Tang et al., 2015; Sun et al., 2015). However, most of those works are on non-reactive particles (i.e., without Stefan flows).

There are also many instances of reacting particles that create a Stefan flow on the particle surface, where the Stefan flow may be due to either heterogeneous reactions or phase change. The flow characteristics (local pressure and velocity, etc.) and interactions (momentum, heat and mass transfer) in particle–fluid flows can vary when a Stefan flow is present. The effect of a Stefan flow on an isolated particle has been studied by many researchers in the past and is summarized in recent work by Jayawickrama et al. (2019, 2021) and Chen et al. (2021). According to the literature, a Stefan flow has a strong effect on the drag coefficient and the heat transfer coefficient through its influence on the thickness of the boundary layer.

There are few studies dedicated to the effects of a Stefan flow on the boundary layer at closely spaced particles in a particle–fluid flow (Chen et al., 2021; Du et al., 2022; Wang et al., 2022). Chen et al. (2021) studied the effect of a Stefan flow on the flow past a random array of spheres. They observed that the effect of a Stefan flow is weakened with increased solid volume fraction. This happens due to suppression of the boundary layer thickening created by an outward Stefan flow compared to an isolated particle. Du et al. (2022) have studied the effect of Stefan flow on the drag force of a single reactive particle surrounded by inert particles. In addition to the observations of Chen et al. (2021), Du et al. (2022) have observed that the reduction of the drag force decreases as Re increases and variation of Re has negligible effects on the reacting particle drag coefficient (C_D) at the solid volume fraction above 0.5. Here, Re is the particle Reynolds number calculated as follows:

$$\text{Re} = \frac{\rho U D}{\mu}, \tag{1}$$

where ρ is fluid density, U is slip velocity between a particle and bulk fluid, D is particle diameter and μ is fluid viscosity. Further, Du et al. (2022) have also developed a model to calculate the drag coefficient for a reacting particle surrounded by a sea of inert particles. Wang et al. (2022) have studied the effect of a Stefan flow on two particles with the Stefan flow in different particle separation and relative orientation between two particles in supercritical water. They have studied $10 \leq \text{Re} \leq 200$, with the distance between two particles in the range of high particle concentrations ($1 \leq L/D \leq 3$) and $0 \leq \text{Re}_{Sf} \leq 3$. Here, the Stefan Reynolds number, Re_{Sf}, is found by replacing U with the Stefan flow velocity, U_{Sf}, in Eq. (1). They observed that the Stefan

flow reduces Nu and C_D. Furthermore, they have found that the drag is significantly impacted by the particle arrangement. In particular, for the same Reynolds number, the combined drag is much lower for particles that are aligned parallel with the flow (tandem) than for particles where the separation vector and the flow are perpendicular (side-by-side). Chen, Du and Wang all have studied quite high solid volume fractions (0.03–0.5), applicable for fluidized-bed conditions. Furthermore, the Reynolds number range studied by Wang et al. (2022) was much greater (Re > 10) than the values observed in conditions relevant for combustion and gasification of pulverized solid fuels (Göktepe et al., 2016a; Saber et al., 2016; Llamas et al., 2022).

All the studies on effects of neighboring particles with Stefan flow (reactive flows) have investigated flows at high particle concentrations that are relevant to fluidized-bed applications ($L/D \leq 3$). Investigations at intermediate and low volume fractions are important for other applications such as pulverized fuel combustion/gasification. García Llamas et al. (2020) have shown that for pulverized biomass gasification, individual particles are likely to interact with only one or a few particles in the vicinity (García Llamas et al., 2020). Therefore, it is important to understand how an isolated pair of reacting particles behaves compared to random arrays of reacting particles. As an example, entrained flow biomass gasification (EFBG) has low particle Re ($0 < \text{Re} \leq 14$) and similar magnitudes of Re_{Sf}. The detailed effects in such conditions have not been studied earlier (most studies like Du et al. (2022) have studied higher ranges of Reynolds number, i.e., Re > 10 and Re $\gg$ Re_{Sf}). Further, none of the studies on the effects of Stefan flow with neighboring particles have investigated the details of pressure and viscous forces and their contribution to the drag coefficient, which is a prerequisite in order to develop a physics-based model describing the effects of Stefan flow and neighboring particles. Since previous particle-pair studies suggest that particles attract each other when they are close enough (Wu and Sirignano, 2011b,a), it is very important to know what happens to these effects when particles experience an outward/inward Stefan flow due to reactions.

Different arrangements of two close particles can be considered as building blocks for arrays with more particles. There are various theoretical, numerical, and experimental studies on the influence of particles located close to each other in different arrangements, like side by side, inline (tandem) and staggered for different Reynolds numbers. The main research findings on tandem arrangement can be summarized as follows (Zhu et al., 1994; Prahl et al., 2009; Wu and Sirignano, 2011b):

  (i) the effect of neighboring particles is weakened at high particle Reynolds number (hereafter, simply referred as Reynolds number),
 (ii) the effect of neighboring particles is less on the *upstream* particle compared to the *downstream* particle,
(iii) the sum of drag on both particles is less than twice the drag of an isolated particle,
(iv) the *upstream* particle drag is always higher than the drag on the *downstream* particle .

Furthermore, Prahl et al. (2007) have shown that the largest change in drag occurs when the particles are in tandem arrangement compared to side-by-side or staggered arrangements. Here, the side-by-side arrangement is when the fluid flow direction and particles' center line are perpendicular to each other. A staggered arrangement is when fluid flow direction and particles' center line are in angles between 0–180 degrees. Kim et al. (1993) have shown that when particles are in a side-by-side arrangement, they repel each other when the particle distance is smaller than a value depending on the Reynolds number. Therefore, these smaller distances can be unstable. At intermediate distances, two particles are weakly attracted to each other.

At very low Reynolds number for the tandem arrangement, upstream and downstream particle drag coefficients will be the same due to the symmetry of the boundary layers. However, the symmetry

is broken already for $Re \geq 0.25$ (Smoluchowski, 1911). For such cases, the decrease in drag coefficients are calculated as a function of particle distance and the Reynolds number ($C_D = \frac{24}{Re}\lambda$ where $\lambda = f(L/D, Re)$) (Stimson and Jeffery, 1926). Recently, Prahl et al. (2007) have shown that the drag coefficient of a particle in tandem arrangement can be calculated as a function of L/D as follows:

$$\frac{C_D}{C_{D,iso}} = 1 - \gamma \left(\frac{L}{D}\right)^{-\beta}, \tag{2}$$

where $C_{D,iso}$ is drag coefficient of an isolated spherical particle, γ is a function of Reynolds number and β is a constant. Raju and Sirignano (1990) and Chiang and Sirignano (1993) have developed models for the drag coefficient of neighboring evaporating droplets. There are no models developed for particles in tandem arrangement with a Stefan flow, as per the authors' knowledge. Therefore, it is important to develop such a model.

This work aims at studying the effect of Stefan flow on closely spaced particles in a uniform flow at a low Reynolds number that is relevant for applications such as pulverized combustion/gasification. The main idea is to isolate the effect of the Stefan flow and the particle separation and, through this, to develop a deep understanding of the variation of the drag coefficient on each particle. The contribution of each force component on the drag coefficient will be studied to obtain the knowledge required to develop physics-based models. This work would then be a starting point for developing such models in the future. To achieve this, two particles inline with each other are considered for different particle Reynolds numbers (Re), Stefan Reynolds numbers (Reynolds number calculated based on Stefan flow velocity (Re_{Sf})) and particle separation (L/D). Particle separations are varied from very close (L/D = 1.1) to intermediate (L/D = 10), which will be applicable for both dense and intermediate solid volume fractions. For this study, we have chosen to focus on the in-line (tandem) particle arrangement. This selection is based on the significant impact the tandem arrangement of neighboring particles has on the drag of particles, both with (Wang et al., 2022) and without Stefan flow (Prahl et al., 2007).

2. Methodology

Numerical simulations were carried out for a flow around two static, spherical particles with constant size in a tandem arrangement (one behind the other as shown in Fig. 1). The incoming gas flow is uniform and isothermal. A uniform Stefan flow is given as a boundary condition at each particle surface. Different cases were simulated by varying the Reynolds number Re $= \rho U_\infty D/\mu$, the Stefan Reynolds number $Re_{Sf} = \rho U_{Sf} D/\mu$ and distance between the two spherical particles (L/D). In these expressions, ρ is the fluid density, U_∞ is the fluid velocity at the inlet boundary of the domain (hereafter referred to as slip velocity), D is the particle diameter, μ is the dynamic viscosity of the fluid, U_{Sf} is the Stefan flow velocity and L is the center-to-center distance between the particles. The Reynolds number is within the limit of steady, axisymmetric flow (Re < 210) (Johnson and Patel, 1999) and the Mach number of the flow is well below 0.1. Therefore, the fluid is governed by the steady, incompressible, laminar flow equations, where mass conservation yields the continuity equation as:

$$\nabla \cdot \vec{u} = 0, \tag{3}$$

and momentum conservation results in,

$$(\rho\vec{u} \cdot \nabla)\vec{u} = -\nabla p + \mu \nabla^2 \vec{u}, \tag{4}$$

where $\vec{u}$ is the velocity vector, p is pressure, μ is dynamic viscosity and ρ is fluid density. Eqs. (3) and (4) are discretized with the finite volume method using second-order schemes. Readers are referred to our previous work for specification of boundary conditions, calculation of Stefan flow velocity and the immersed boundary method (Jayawickrama et al., 2019). The only difference is that, there are now two solid particles in tandem instead of one.

Table 1
Parameter variation in the simulations.

Slip velocity U_∞ (m/s)	Particle diameter D (mm)	Particle separation L/D	Reynolds number Re
0.5	1.0	1.1, 1.5, 2.5, 5.0, 7.5, 10.0	2.3
3.0	0.5	1.1, 1.5, 2.5, 5.0, 7.5, 10.0	7
3.0	1	1.1, 1.5, 2.5, 5.0, 7.5, 10.0	14

Table 2
The sizes and resolutions of the refinement regions in the computational domain (See Fig. 1).

i	$D_{-x,i}$	$D_{+x,i}$	$D_{y,i}, D_{z,i}$	Δ_i/D
1	16	48	32	0.32
2	3	6	3	0.16
3	2	5	2	0.08
4	1.5	3	1.5	0.04
5	1.2	2	1.2	0.02

2.1. Simulation conditions

The slip velocity (relative velocity between a particle and the bulk fluid), particle diameter and Stefan flow velocities for the simulations were selected based on pulverized combustion and entrained flow gasification conditions at atmospheric pressure (Umeki et al., 2012; Llamas et al., 2022). Details of velocity, diameter and distance between particles are shown in Table 1. The Stefan flow velocity was estimated based on data from devolatilization and char conversion of biomass (Kreitzberg et al., 2016; Umeki et al., 2012). Three values of the Stefan flow velocity were considered, namely $U_{Sf} = -0.2$ m/s (inward Stefan flow), 0 m/s (no Stefan flow) and 0.6 m/s (outward Stefan flow). The Reynolds numbers are 2.3, 7 and 14. Since the Reynolds number is less than 20 in this study, the flow is steady and axisymmetric (Johnson and Patel, 1999). Therefore, only a quarter of the domain was simulated while symmetric boundary conditions were used at the boundaries with the other three parts.

We used the OpenFoam environment, called *foam-extend*-4.0 (Weller et al., 1998). The numerical simulations were carried out using the same solver as in Jayawickrama et al. (2019); the incompressible, steady-state, immersed boundary code.

Based on the domain size and mesh refinement tests (see Appendix), simulations presented in this work used domain 3 as defined in Table A.4, mesh refinement of the smallest mesh close to the particle of 0.02D (Level 5 in Fig. 1) and the mesh refinement region sizes as shown in Table 2. Fig. 1 shows the details of the domain and mesh refinement regions used for all the simulations. A validation of the code used for the numerical simulations can be found in Jayawickrama et al. (2019).

2.2. Estimation of the drag coefficient

The drag coefficient is calculated as (Jayawickrama et al., 2019):

$$C_D = \frac{F_{P,x} + F_{visc,x}}{\frac{1}{2}\rho U_\infty^2 (\pi R^2)}, \tag{5}$$

where the pressure and viscous forces are given as

$$\vec{F}_P = \oint_S (P_{sur} - P_{ref})\vec{n}\, ds, \tag{6}$$

and

$$\vec{F}_{visc} = -\oint_S \mu(\nabla \vec{u} + \nabla \vec{u}^t)\vec{n}\, ds, \tag{7}$$

respectively. Here, the integration is over the surface S of the particle. In the above, P_{sur} and P_{ref} are the interpolated pressure at the particle surface and in the far-field, respectively, and $\vec{n}$ is the unit vector in the surface-normal direction. Only the components $\vec{F}_P$ and $\vec{F}_{visc}$ in the direction of the mean flow were accounted for when calculating the drag coefficient, since the other components are canceled out due to symmetry.
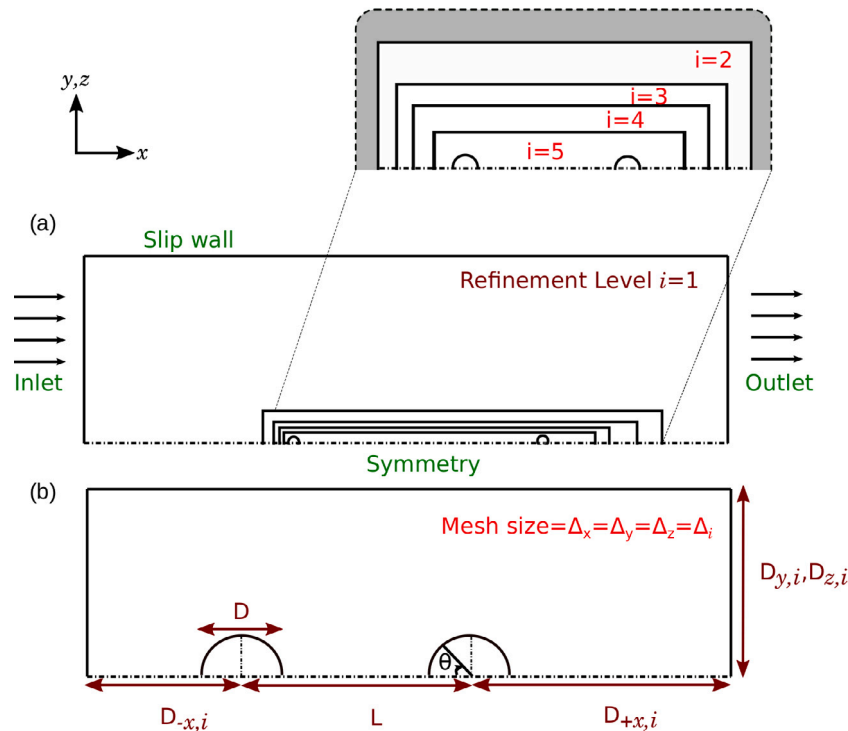
Fig. 1. Computational domain for the simulations, with D denoting the particle diameter, and Δ_i, $i = 1$ to 5 representing the coarsest to finest mesh. $D_{-x,i}$ is the distance from the center of the first sphere to the inlet and $D_{+x,i}$ is the distance from the center of the second sphere to the outlet (See Table 2). $D_{y,i}$ is the distance from the symmetry line to the boundary in the lateral direction.

3. Results and discussion

In this work, we have made a parameter study on the effect of two closely spaced particles on the surrounding fluid flow. The parameters are: (1) Stefan flow velocity (including direction), (2) Reynolds number, and (3) inter-particle distance. First, the effect on the boundary layer is shown through the velocity and pressure fields. Streamlines of the gas velocity are also studied around the two particles. Then, the total pressure and viscous forces on the two particles are investigated to clarify the contribution of each component on the total drag. Pressure and viscous forces are also presented at different positions around the particles to see how the effect of the Stefan flow vary with particle separation at different angular positions.

3.1. Variations on the pressure and velocity fields

3.1.1. Without Stefan flow

Fig. 2 shows the relative pressure field around two neighboring particles with different separations for the case without a Stefan flow. The distance between the two particles is represented by the ratio of particle distance to particle diameter (hereafter, L/D ratio). Both *upstream* and *downstream* particles show regions with positive relative pressure in front of the particle and regions with negative relative pressure behind the particle. The effects of the *upstream* particle are visible on the *downstream* particle for all the L/D ratios considered in this work. The positive pressure region of the *downstream* particle shrink as the L/D ratio is lowered, while the negative pressure region display almost no difference. When $L/D < 2.5$, the pressure field around the *downstream* particle has just a very small area with positive pressure. Effects of the *downstream* particle on the *upstream* particle are visible for $L/D < 7.5$. Here, the positive pressure region is hardly affected while the negative pressure region behind the particle is reduced for decreasing particle separation.

Fig. 3 shows the velocity contours in the mean flow direction around the particles without Stefan flow. Judging from the outer contour

line for 0.8 U_∞, the width of the velocity boundary layer reaches a maximum somewhere after the *downstream* particle. This maximum boundary layer width is slightly smaller for the low L/D ratio. As the L/D ratio decreases, the boundary layers of the two particles start merging. At $L/D \leq 1.5$, the velocity boundary layers from the two particles merge and resemble the boundary layer around one particle. There is no flow, or negligible fluid flow, between the particles.

3.1.2. With outward Stefan flow

Fig. 4 compares the contour plots of velocity (in the mean flow direction) with and without outward Stefan flow. A clear difference is shown between the cases with and without a Stefan flow. There is a shared boundary layer between the two particles in all cases with an outward Stefan flow considered in this work. An outward Stefan flow makes the size of this boundary layer significantly larger. This could potentially lower the drag force on the particles compared to the drag previously found for an isolated particle (Jayawickrama et al., 2019).

The outward Stefan flow acts as a shield against the bulk flow and makes the velocity profiles around the two particles independent from each other. Streamlines shown in Fig. 5 clearly depict this shielding effect of the Stefan flow around the two particles. It shows the stagnation point between the two particles, which coincides with the point where the velocity magnitude is zero, as also shown in Fig. 4. These observations suggest that the effect of neighboring particles on the viscous force may become less important with the presence of an outward Stefan flow.

3.1.3. With inward Stefan flow

Figs. 6 and 7 compares velocity contours (in the mean flow direction) and streamlines for cases with inward Stefan flow and without Stefan flow. Contrary to the case with outward Stefan flow, an inward Stefan flow makes the size of the boundary layer significantly smaller, both in width and length. This results in a steeper velocity gradient, potentially yielding a larger viscous force and thereby also a larger drag.
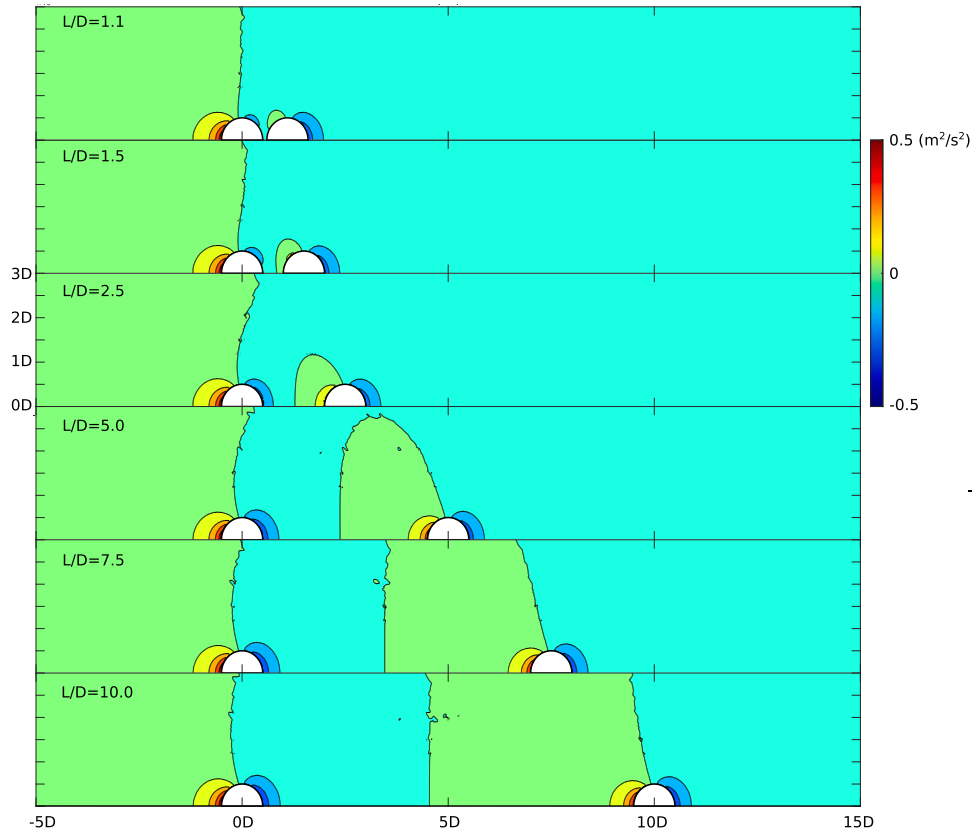
Fig. 2. Pressure contours around particles with no Stefan flow and $Re = 2.3$. Pressure is shown as the difference from the reference pressure at the domain outlet. The color map is adjusted to display positive pressure in green-to-red ranges and negative pressure in green-to-blue ranges. (For interpretation of the references to color in this figure legend, the reader is referred to the web version of this article.)
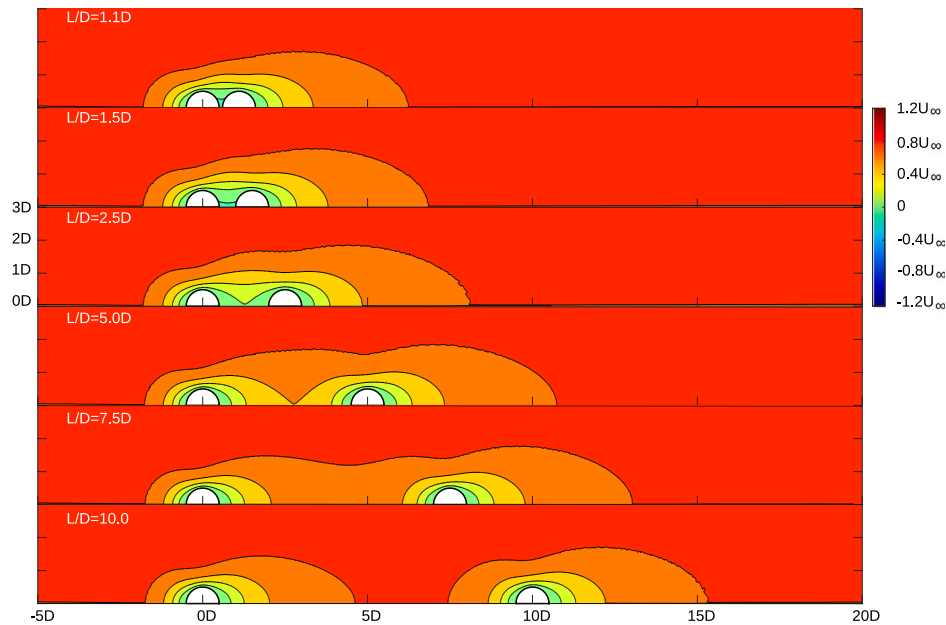

Fig. 3. Velocity contours in the mean flow direction around the particles when there is no Stefan flow around the particle at $Re = 2.3$. Here contours start from $0U_\infty$, contour intervals are in $0.2U_\infty$ and far-field velocity is $1U_\infty$.

No obvious shielding effect between the two particles was observed with an inward Stefan flow. Inward Stefan flows have much smaller effects on the streamlines outside the particles. With inward Stefan

flow, the zero velocity zone surrounding the particle surface disappeared. Nevertheless, mergers of the boundary layers of two particles were avoided with inward Stefan flow at low L/D ratios (See Fig. 6,
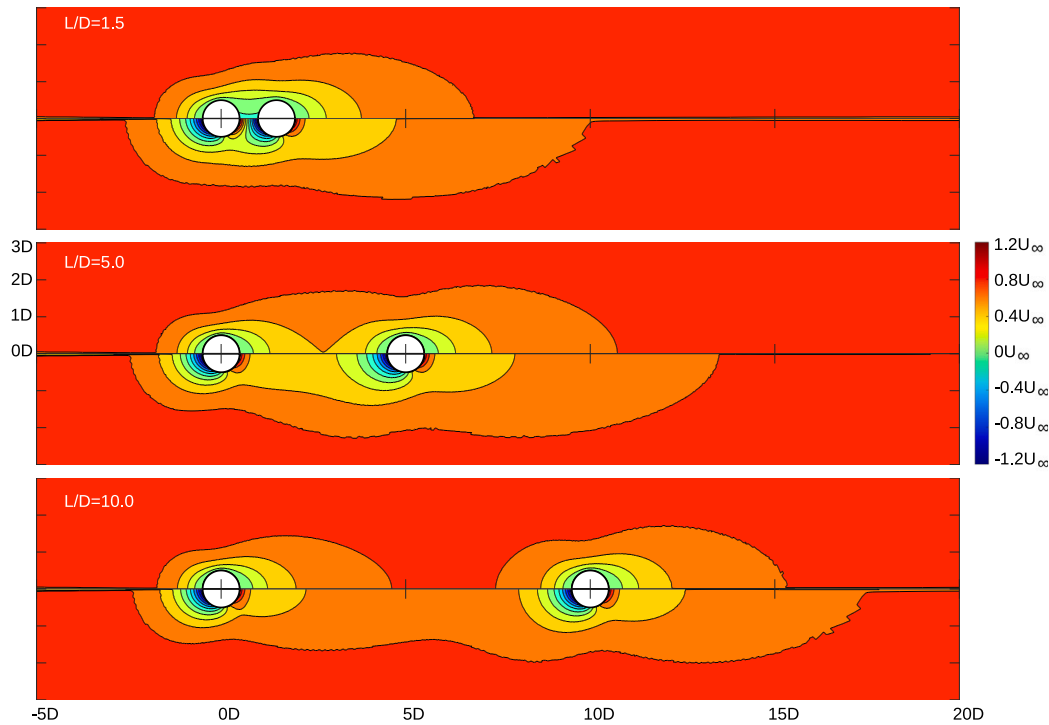
Fig. 4. Velocity contours in the mean flow direction around the particles with $Re = 2.3$. The top half of each panel shows the cases without Stefan flow while the bottom half is cases with outward Stefan flow ($U_{Sf} = 0.62$ m/s corresponding to $Re_{Sf} = 2.9$). Here contours start from $0U_{\infty}$, contour intervals are in $0.2U_{\infty}$ and far-field velocity is $1U_{\infty}$.

$L/D = 1.5$). These observations imply the presence of an additional effect of Stefan flow with small particle distances (i.e. $L/D < 1.5$).

For inward Stefan flow, there is a separating streamline; flow inside this separating streamline ends up at the particle surface while flow outside will pass the two particles. Due to symmetry, the vertical distance y_{∞} of this separating streamline follows as $y_{\infty} = (2U_{Sf}/U_{\infty})^{1/2}D$.

3.2. Drag coefficient

Fig. 8 shows the effect of the L/D ratio on the relative drag coefficient, normalized with the value of an isolated particle without Stefan flow. Here, the normalization coefficient corresponding to the drag coefficient of an isolated particle without Stefan flow is found from our previous work (Jayawickrama et al., 2019). It can also be calculated from Haider and Levenspiel model (Haider and Levenspiel, 1989):

$$C_d = \frac{24}{Re}(1 + 0.1806Re^{0.6459}) + 0.4251(1 + \frac{6880.95}{Re})^{-1}. \quad (8)$$

The data is shown for various Reynolds numbers and Stefan Reynolds numbers. The drag coefficient of two neighboring particles with a Stefan flow is clearly different from the drag coefficient of an isolated particle with a Stefan flow alone (mimics a reacting isolated particle) and the drag coefficient of two neighboring particles without a Stefan flow (mimics a non-reacting particle surrounded by other particles). Downstream particles have a lower drag coefficient than isolated particles even at the largest particle distance investigated in this study (i.e., $L/D = 10$). The drag of *downstream* particles is affected more significantly by *upstream* particles at a higher Reynolds number. The drag coefficient of *upstream* particles starts dropping when the particle distance is below $L/D \leq 5$, although this limit depends on the Reynolds number.

These results also agree with other studies (Prahl et al., 2009; Wu and Sirignano, 2011b), i.e., when two particles are in tandem arrangement with another particle, both particles' drag coefficients are less than that of an isolated particle.

The effects of a Stefan flow can be seen by comparing the central figures of Fig. 8 (b,e,h) with the figures to the left (inward Stefan flow)

and the right (outward Stefan flow). In general, for $L/D \geq 2.5$, the results agree with the previous studies (Jayawickrama et al., 2019; Kékesi et al., 2019), that is, an outward (inward) Stefan flow decreases (increases) the drag coefficient. Except for the cases with $L/D < 2.5$, the drag coefficients of both *upstream* and *downstream* particles showed a similar response to changes in the L/D ratios. As the L/D ratio increases, the drag coefficients of *upstream* particles become asymptotic to those of isolated particles with the same combinations of Re and Re_{Sf}. Although it is slowly approaching the asymptotic values, the drag coefficient of *downstream* particles do not reach that of isolated particles before $L/D = 10$. Stefan flow and neighboring particles seem to affect the drag independently for $L/D > 2.5$.

When the two particles are very close ($L/D < 2.5$), an outward Stefan flow increases the drag of *downstream* particle and reduces the drag of *upstream* particle significantly. This makes the drag of a *downstream* particle exceed that of an *upstream* particle. The point where this change happens depends on the Reynolds number and potentially on the Stefan flow velocity as well. As shown in Fig. 8 (c,f,i), the effect is more significant at a lower Reynolds number. At $Re = 2.3$ and $L/D = 1.1$, the *upstream* particle experienced negative drag, meaning that the net force on the particle is working against the bulk flow direction. At the same time, the drag ratio of the *downstream* particle exceeded one. This can be explained by the results discussed in Section 3.1 (Figs. 2 and 3). When $L/D < 1.5$, the two particles behaved like a single particle, and no flow from the bulk gas was observed between the particles. Therefore, the Stefan flow effect alone comes into play in the volume between the two particles. The outward Stefan flow then results in high pressure and a large velocity gradient between two particles. As a result, the two particles repulse each other. This effect act in the opposite direction on the two particles but with the same magnitude, as shown in Fig. 8.

The effect of inward Stefan flow shows two distinct regimes based on the L/D ratios, similar to what was observed for outward Stefan flow. At high L/D ratios, the effects of Stefan flow and neighboring particles were independent of each other. At small particle distances ($L/D < 1.5$), an inward Stefan flow increases the drag of the *upstream*
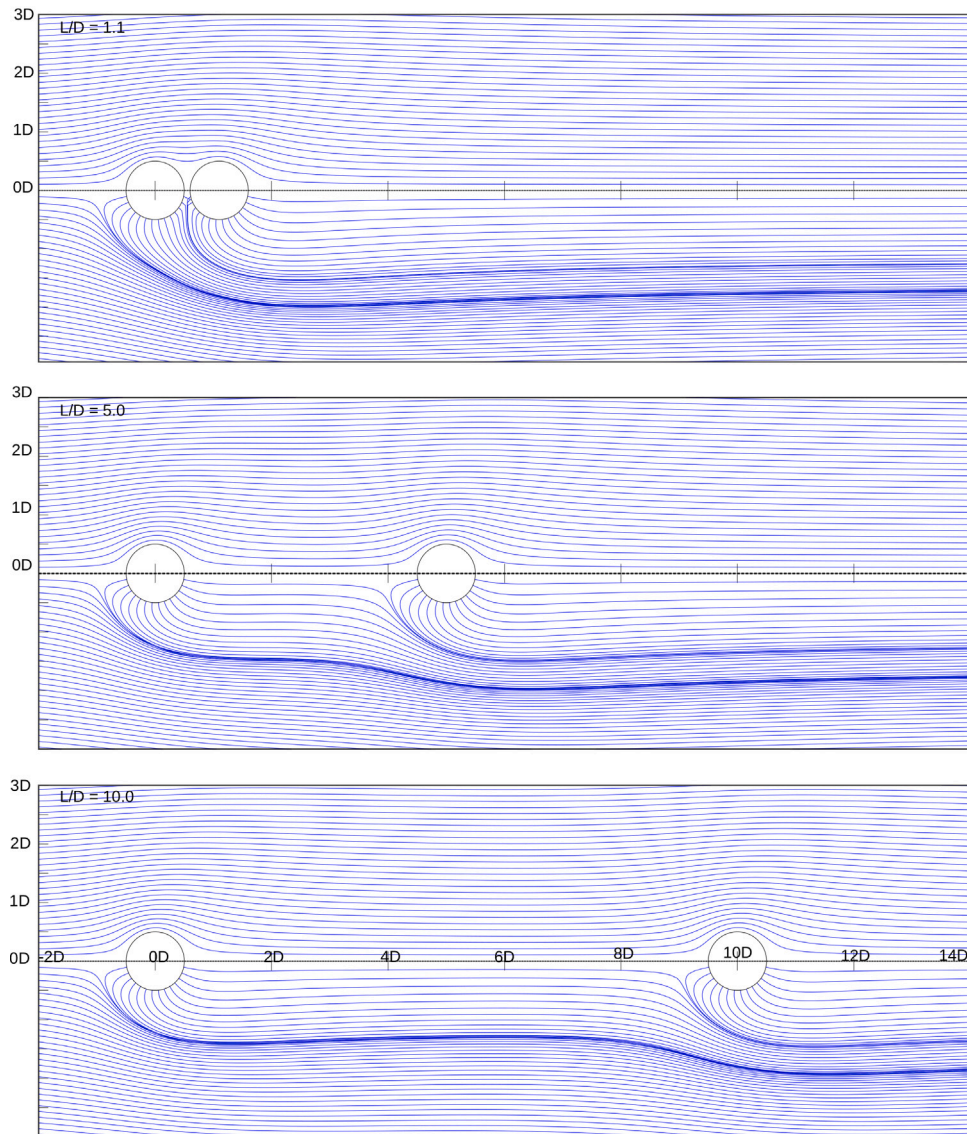
Fig. 5. Streamlines surrounding the particles at $Re = 2.3$. The top half of each panel corresponds to the case without Stefan flow while the bottom half represents the case with outward Stefan flow ($U_{Sf} = 0.62$ m/s corresponding to $Re_{Sf} = 2.9$).

particle and reduces that of the *downstream* particle considerably. This transition is similar to the one observed with outward Stefan flow, but the force is in the opposite direction, i.e., the two particles attract each other.

In most cases shown in Fig. 8 (except for $L/D < 1.5$), the drag coefficient of the *upstream* particle is always higher than that of the *downstream* particle and both *upstream*, and *downstream* particle drag coefficients are positive (drag is in the mean flow direction). Hence, the distance between two particles in tandem will decrease with time if the two particles can move freely. Without a Stefan flow, it is expected that the two particles will eventually collide and either form aggregates or bounce off each other. However, repulsive forces via an outward Stefan flow will become significant at low L/D ratios. Especially at low Reynolds numbers (at least at Re ≤ 14), this force may overcome the inertia, and particles may not come into physical contact. On the other hand, inward Stefan flows enhance the differences between the drag coefficients of the two particles and accelerate the attraction between them.

The relative importance of inertia over the viscous force increases at a higher Reynolds number, resulting in thinner boundary layers. Similarly, the expansion of the boundary layer by an outward Stefan flow becomes less significant at higher particle Reynolds numbers. This difference can be observed by the distance to the stagnation point, as visualized in Fig. 5. As shown in Fig. 9, the stagnation distances significantly decrease as the Reynolds number increases. In addition, downstream particles exhibit longer stagnation distances than upstream particles, and this effect is enhanced as the particles come closer. Since the stagnation distance of the downstream particle cannot exceed the particle separation, high pressure and viscous forces are generated when the particle separation approaches the stagnation distances.

3.3. Viscous and pressure forces

3.3.1. Overall forces

Figs. 10 and 11 show total pressure force and viscous force on the particles for the same conditions as in Fig. 8. Both total viscous and total pressure forces have similar trends as those observed for the drag coefficients. The forces are reduced as the particle distance decrease (except for $L/D < 1.5$). An outward Stefan flow lowers the viscous force, while an inward Stefan flow increases the force. At $L/D < 1.5$, the effect of a Stefan flow on the forces differs from $L/D > 1.5$. For example, *downstream* particle viscous and pressure forces start to
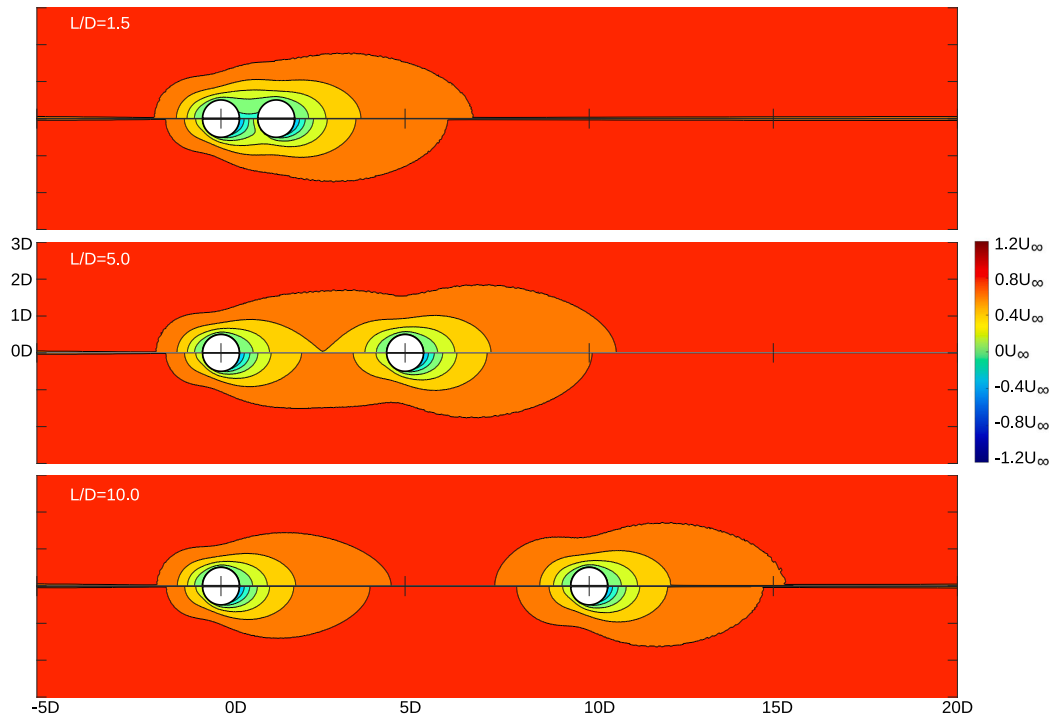
Fig. 6. Velocity contours in the mean flow direction around the particles at $Re = 2.3$. The top half of each figure is the velocity in the case without Stefan flow and the bottom half is the case with inward Stefan flow ($Re_{Sf} = -0.96$). Here contours start from $0U_\infty$, contour intervals are in $0.2U_\infty$ and far-field velocity is $1U_\infty$.

increase at $L/D < 1.5$ with an outward Stefan flow instead of following the decreasing trend observed for $L/D > 1.5$ (Figs. 10 and 11 c,f,i). The same effect can be observed on the *upstream* particle with an inward Stefan flow (Figs. 10 and 11 a,d,g).

Meanwhile, the relative changes in pressure and viscous force are quantitatively different from each other. Effects of neighboring particles can be observed more profoundly on pressure forces, judging from larger differences in the pressure forces between *upstream* and *downstream* particles. The effect of Stefan flow at low particle distance ($L/D = 1.1$) is also more notable in pressure force. With an outward Stefan flow, the normalized pressure force of the *downstream* particle is as high as 4 and that of the *upstream* particle is negative (≈ -3). The normalized viscous force at the same condition is about 1.5 for the *upstream* particle and about -0.5 for the *downstream* particle. The effect is less significant at a higher Reynolds number. Similarly, the effect of an inward Stefan flow at $L/D = 1.1$ is more visible in the pressure force than in the viscous force.

The effects of a Stefan flow for $L/D > 1.5$ is more profound on the viscous force. Compared to the middle panels (Fig. 11 b,e,h), viscous force is shifted upwards for the left panels (Fig. 11 a,d,g) and downward for the right panels (Fig. 11 c,f,i). This means that an outward Stefan flow reduces viscous force while an inward Stefan flow increases viscous force. This behavior agrees with previous studies (Jayawickrama et al., 2019). The uniform Stefan flow velocity controls the velocity field around the particle and shifts the boundary layer away from the surface (See Fig. 4 all the bottom figures), which reduces the viscous force on the particle. A deviation from this trend occurs when particles are very close. The reason is a total or partial blocking of the fluid flow between the particles. The Stefan flow will create high pressure and steep velocity gradients in that region, which affects the viscous and pressure forces.

3.3.2. Pressure and viscous stress at different angles

At both Reynolds numbers considered in Figs. 12 and 13, the local pressure force is higher than the local viscous force, i.e., the effect of a neighboring particle is mainly on the pressure force. When $Re = 2.3$

and $L/D = 1.1$, equal and opposite values of the viscous and pressure forces are observed at the back of the *upstream* particle and at the front of the *downstream* particle ((a) and (b) of Fig. 12). These equal and opposite forces are observed only in the pressure force for $Re = 14$ and $L/D = 1.1$ ((a) of Fig. 13). The effect of neighboring particles on the viscous force is not clear for $Re = 2.3$ and $L/D \geq 5$ ((d) and (f) of Fig. 12). However, the effect of neighboring particles on the viscous force is clearly visible at $Re = 14$ and $L/D \geq 5$ ((d) and (f) of Fig. 13). There is a clear net negative viscous force (repulsive) on the *upstream* particle with an outward Stefan flow when $Re = 2.3$ and $L/D = 1.1$. This is due to the high velocity gradients between the particles due to an outward Stefan flow with a velocity magnitude greater than the far-field velocity ($U_{Sf} > U_\infty$).

As we have observed from our previous work, for a single spherical particle, the effect of Stefan flow mainly affects the viscous force, but not the pressure force, at $Re < 14$ (Jayawickrama et al., 2019). However, Stefan flow effects are visible on the pressure force of the *downstream* particle ((c) and (e) of Figs. 12 and 13) as well. Therefore, the existence of a particle in *upstream* changes the effect of a Stefan flow on the *downstream* particle, or the relevance of a Stefan flow depends on the distance to other particles.

3.4. Drag model

Based on the above observation, a model was developed for the drag coefficient of two closely spaced particles with Stefan flow. The model consists of individual models describing: (1) the effects of a Stefan flow on the particle itself, $C_{D,r,Sf}$, (2) the effects of neighboring particles, $C_{D,r,up,noSf}$ and $C_{D,r,dp,noSf}$, including (3) repulsive/attractive forces due to a Stefan flow at very low L/D, and (4) the effects of Stefan flow from the upstream particle on the downstream particle, $C_{D,r,Sf2}$. The drag coefficients of the upstream particle, $C_{D,up}$, and downstream particle, $C_{D,dp}$, are expressed as the product of these individual models as:

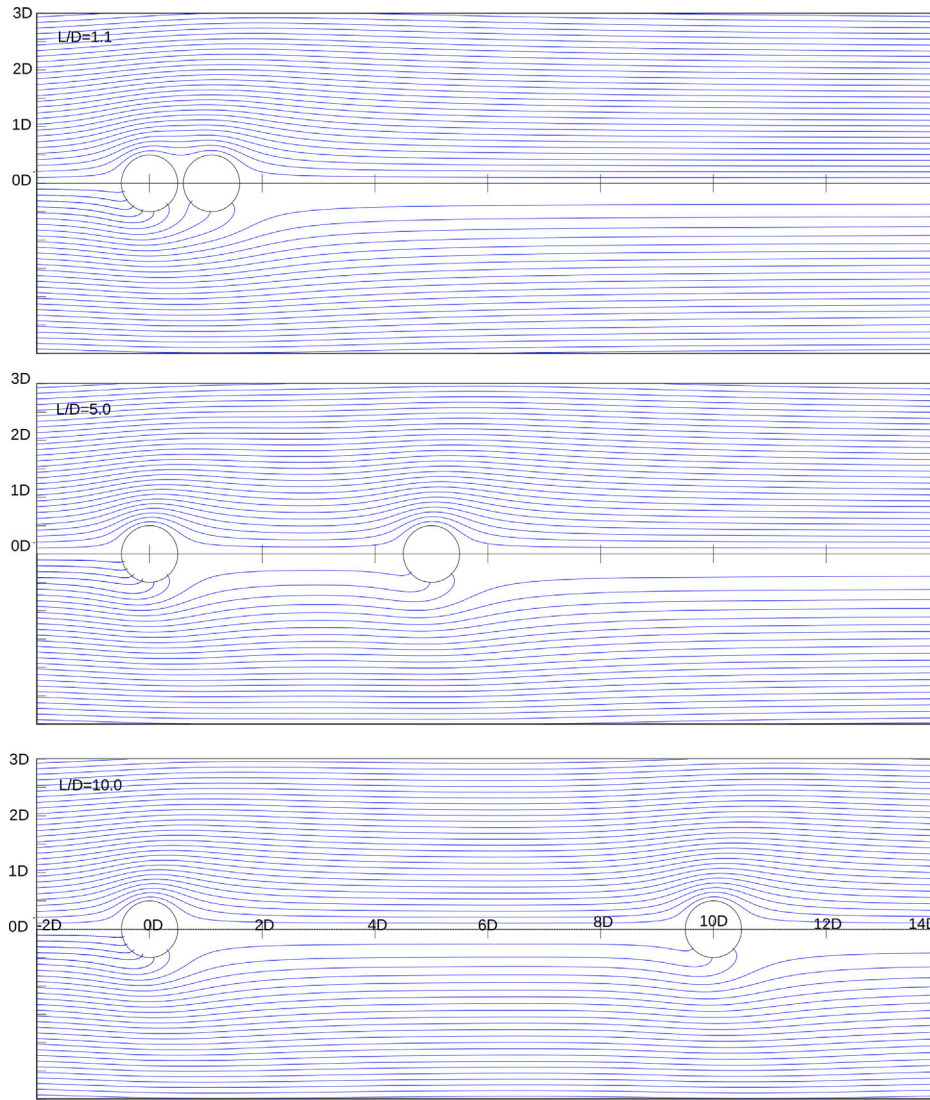$$C_{D,up} = C_{D,0} \cdot C_{D,r,Sf} \cdot C_{D,r,up}, \tag{9}$$

Fig. 7. Streamlines surrounding the particles at $Re = 2.3$. The top half of each figure is the case without Stefan flow and the bottom half is the case with inward Stefan flow ($Re_{Sf} = -0.96$). Streamlines are uniform in the incoming flow but due to the inward Stefan flow condition where volume flow rate interior to the particle depends on R^2, *downstream* particle reaches less number of streamlines.

and

$$C_{D,dp} = C_{D,0} \cdot C_{D,r,Sf} \cdot C_{D,r,dp} \cdot C_{D,r,Sf2}, \tag{10}$$

where $C_{D,0}$ is the drag coefficient of an isolated particle without Stefan flow, calculated from e.g. the Haider and Levenspiel model (Haider and Levenspiel, 1989) (cf. Eq. (8)), and $C_{D,r,up}/C_{D,r,dp}$ is the drag ratio due to the effects of neighboring particles ($C_{D,r,up,noSf}/C_{D,r,dp,noSf}$) along with repulsive/attractive forces due to a Stefan flow at very low L/D (see Eq. (13) - (16)).

A model for the effect of Stefan flow on an isolated particle was developed in our previous work (Jayawickrama et al., 2019), and expressed as:

$$C_{D,r,Sf} = \frac{1}{1 + f(\text{Re})\text{Re}_{Sf}}, \tag{11}$$

with

$$f(\text{Re}) = \frac{3}{\text{Re}}(1 + \frac{2A}{\sqrt{\text{Re}}}) \frac{1}{(\frac{3A}{\sqrt{\text{Re}}} + 6(\frac{A}{\sqrt{\text{Re}}})^2 + 4(\frac{A}{\sqrt{\text{Re}}})^3)}. \tag{12}$$

The parameter from our previous work, $A = 3.01 \pm 0.13$, was applied without any modification.

As discussed in Section 1, Prahl et al. (2007) suggested a model to calculate the drag coefficient of particles in tandem arrangement (Eq. (2)). The simulation data without Stefan flow (Fig. 8 b, e, and h) was used to estimate the parameters in this model. To avoid excessive parameter fitting, $\beta = -1$ was applied for the upstream particle, while $\beta = -0.5$ was used for the downstream particle. As a result, the effect of neighboring particles without Stefan flow was expressed as:

$$C_{D,r,up,noSf} = 1 - 0.321\text{Re}^{-0.235} \left(\frac{\text{L}}{\text{D}}\right)^{-1}, \tag{13}$$

for the upstream particle and

$$C_{D,r,dp,noSf} = 1 - 0.390\text{Re}^{0.151} \left(\frac{\text{L}}{\text{D}}\right)^{-0.5}, \tag{14}$$

for the downstream particle.

At very low L/D, a positive (negative) Stefan flow generated a repulsive (attractive) force between the two particles. This force acts on both particles with the same magnitude, but in opposite direction. To account for this force an additional term is added to Prahl's model, such that the final expressions that enter Eqs. (9) and (10) read as

$$C_{D,r,up} = 1 - 0.321\text{Re}^{-0.235} \left(\frac{\text{L}}{\text{D}}\right)^{-1} - \alpha \left(\frac{\text{L}}{\text{D}} - 1\right)^{-1}, \tag{15}$$
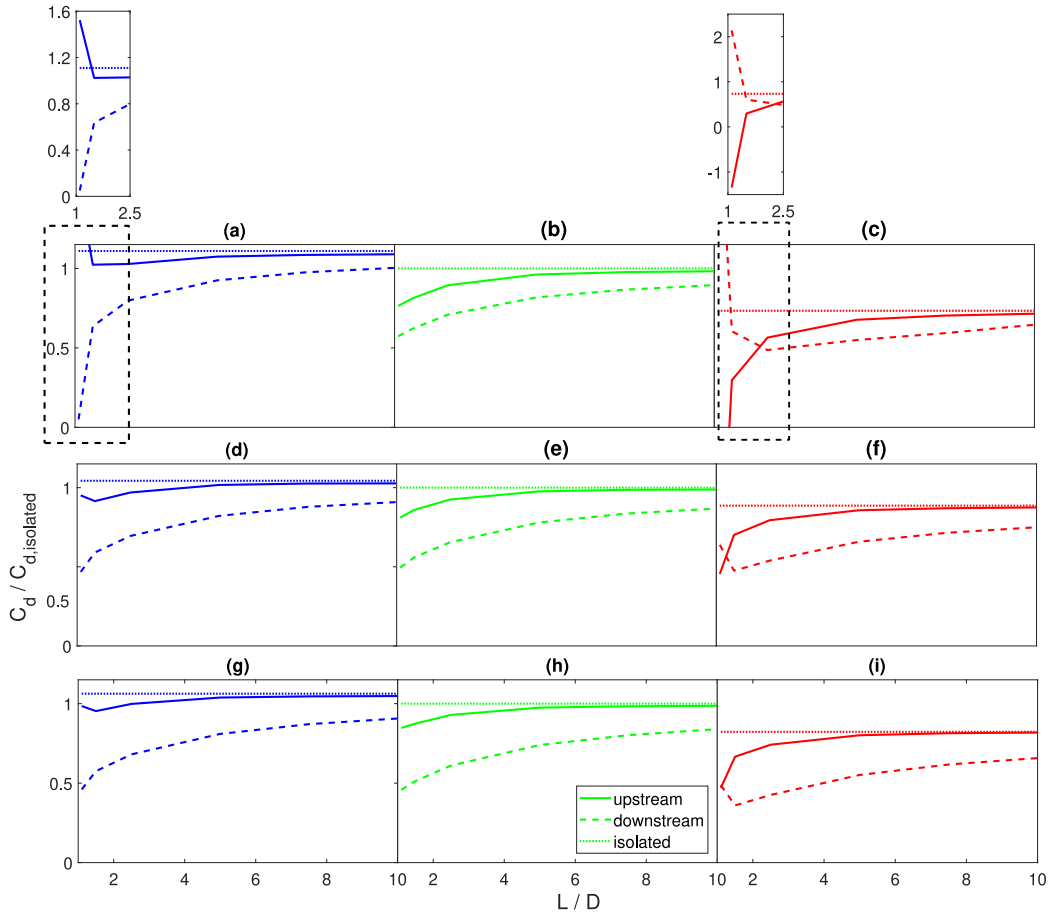
Fig. 8. Relative drag coefficient, normalized with the value of an isolated particle without Stefan flow, as a function of the particle separation (L/D). (a-c) $Re = 2.3$; (d-f) $Re = 7$; (g-i) $Re = 14$. (a,d, (g) $U_{Sf} = -0.2$ m s^{-1}; (b,e, (h) $U_{Sf} = 0$ m s^{-1}; (c,f, (i) $U_{Sf} = 0.6$ m s^{-1}. The drag coefficient of an isolated particle without Stefan flow can be calculated using the model of Haider and Levenspiel (1989): $C_d = \frac{24}{Re}(1 + 0.1806 Re^{0.6459}) + 0.4251(1 + \frac{6880.95}{Re})^{-1}$.
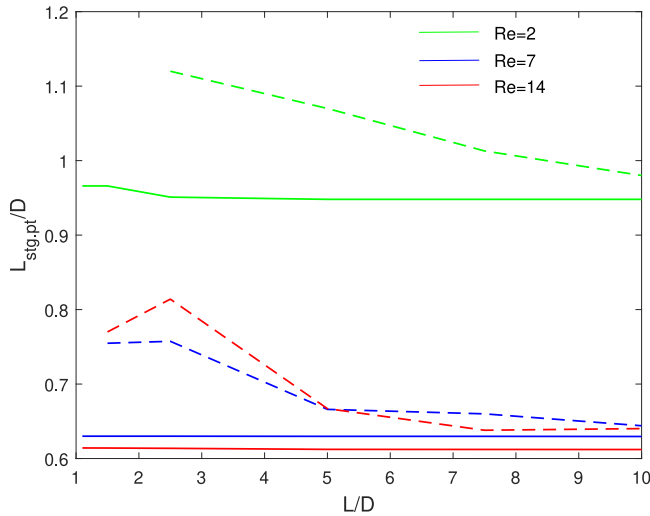
Fig. 9. Stagnation point distance from the center of upstream and downstream particle for each Re and L/D with outward Stefan flow ($U_{Sf} = 0.6$ m/s). Solid lines represent upstream particles, and dashed lines represent downstream particles.

and

$$C_{D,r,dp} = 1 - 0.390 Re^{0.151}\left(\frac{L}{D}\right)^{-0.5} + \alpha\left(\frac{L}{D} - 1\right)^{-1}, \quad (16)$$

respectively. Here, the repelling/attracting force exist due to high pressure at the stagnation point between two particles. Therefore, based on Bernoulli equation, the force should be proportional to U_{Sf}^2. Considering the definition of the drag coefficient (Eq. (5)), the term, α, is approximated as:

$$\alpha = b_1 \left(\frac{Re_{Sf}}{Re}\right)^2 + b_2 \frac{Re_{Sf}}{Re}. \quad (17)$$

where b_1 and b_2 are fitting parameters.

Finally, there is an additional interparticle effect of Stefan flow because a Stefan flow from an upstream particle causes expansion or shrinkage of the boundary layer of the downstream particle. This additional expansion/shrinkage effect that affects the downstream particle is modeled in a similar way as the effect of Stefan flow on a single particle. In other words, the last term in Eq. (10), i.e. $C_{D,r,Sf2}$ that accounts for this expansion/shrinkage effect, is described by Eqs. (11) and (12) with the constant A replaced by a separate fitting parameter, B.

Three model parameters, b_1, b_2, and B, were estimated by minimizing the root mean square relative error (RMSRE) between the simulation data and the model results using *fminsearch* function in matlab. RMSRE is expressed as:

$$RMSRE = \sqrt{\frac{\Sigma\left[\frac{(C_{D,sim} - C_{D,model})}{C_{D,sim}}\right]^2}{N}}, \quad (18)$$

where $C_{D,sim}$ is the drag coefficient values from the simulations and $C_{D,model}$ is the drag coefficient values calculated from the model.
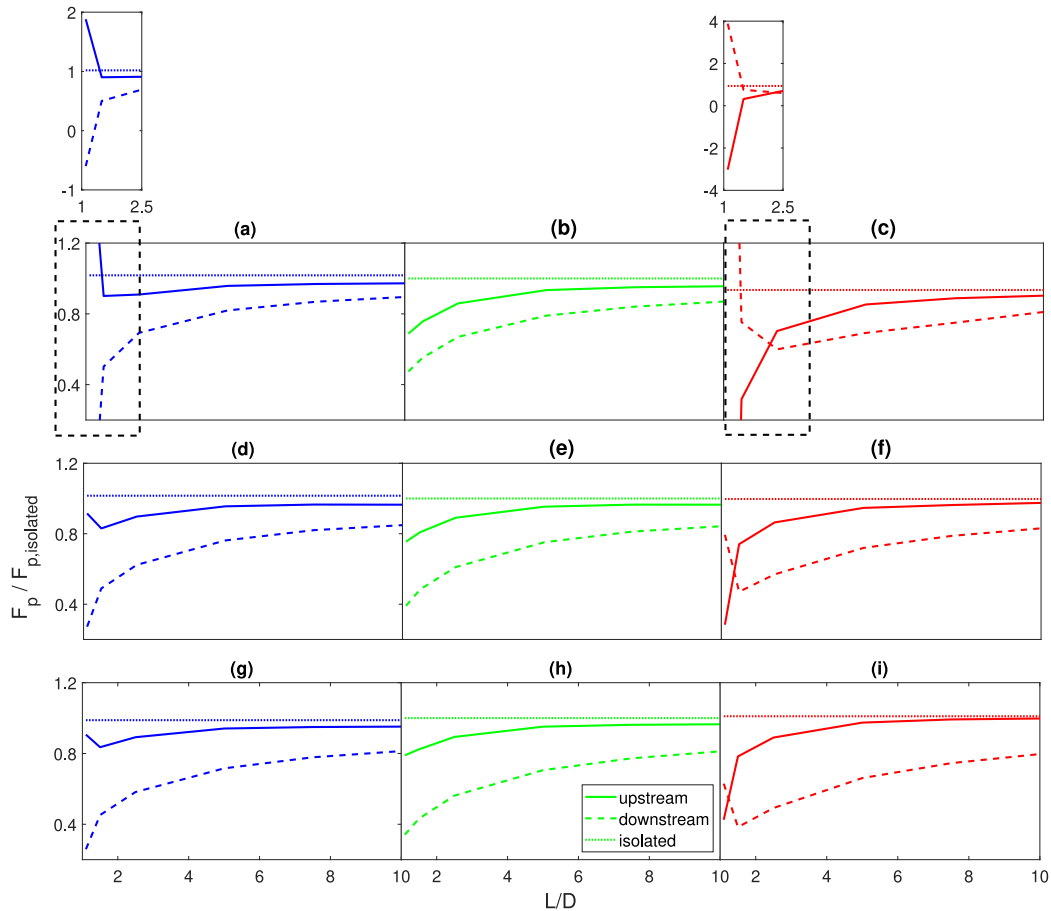
Fig. 10. Total pressure force, normalized with the value of an isolated particle without Stefan flow, as a function of the distance between particles (L/D). (a-c) $Re = 2.3$; (d-f) $Re = 7$; (g-i) $Re = 14$. (a,d, (g) $U_{Sf} = -0.2$ m s^{-1}; (b,e, (h) $U_{Sf} = 0$ m s^{-1}; (c,f, (i) $U_{Sf} = 0.6$ m s^{-1}.

Fig. 14 shows the comparison of the simulation results and the model given by Eqs. (9) and (10) with the estimated parameters shown in Table 3. It shows a good agreement between the model and the simulation results. The overall RMSRE is 0.0499 while the value for the upstream particle is 0.0238 and that for the downstream particle is 0.0665. The model developed here has in total 8 parameters (5 for the upstream particle and 6 for the downstream particles, of which 3 parameters are shared). However, we should note that the model is a combination of several independent models, which are based on physical observation and have only one or two parameters each. The model for Stefan flow effects by Jayawickrama et al. (2019) (Eqs. (11) and (12)) was directly adopted including the parameter value. The model for the effects of neighbor particles are based on previously developed models by Prahl et al. (2007) with their parameters fitted with the simulation data without Stefan flow. On top of that, a model describing the equal and opposite force by the Stefan flow that is apparent at $L/D \leq 2.5$ was developed in this work (see Eq. (15) and (16)). This has introduced two new model coefficients b_1 and b_2 (see Eq. (17)). The overall model is robust and versatile because each model component describes an individual physical effect with a minimal number of fitting parameters.

4. Conclusions

In this study, we have carried out particle-resolved numerical simulations for two reacting particles in tandem arrangement with different distances between the particles. Reaction generated flow (Stefan flow)

Table 3
Estimated parameters of the drag model.

Parameters	b_1	b_2	B
Values	0.0332	0.1426	3.546

is considered either outward/inward uniform flow from/to the particle. Particle Reynolds number (Re), Stefan flow (Re_{Sf}) and particle distance has varied during simulations.

Without Stefan flow, the effect of an *upstream* particle on the *downstream* particle is not negligible for any of the particle distances and Reynolds numbers considered in this work ($Re = 2.3 - 14$ and $L/D = 1.1 - 10$). The effect of a *downstream* particle on the *upstream* particle can, however, be neglected when $L/D > 5$. When particles are very close to each other, the fluid flow between the particles is totally ($L/D < 1.5$) or partially ($1.5 < L/D < 2.5$) blocked by the *upstream* particle.

The combined effects of a Stefan flow and neighboring particles on the drag coefficient seem to work independently without any interaction for $L/D > 2.5$. An outward Stefan flow decreases the drag coefficients compared to the cases without a Stefan flow, while an inward Stefan flow increases drag coefficients. Similar to the effects on isolated particles, the effect of an outward Stefan flow on the drag coefficient can be explained by the expansion of the boundary layer and the accompanying decrease in viscous force.

A deviation from the previous observations occurs when $L/D < 2.5$ since the fluid flow is blocked between the *upstream* and the *downstream*
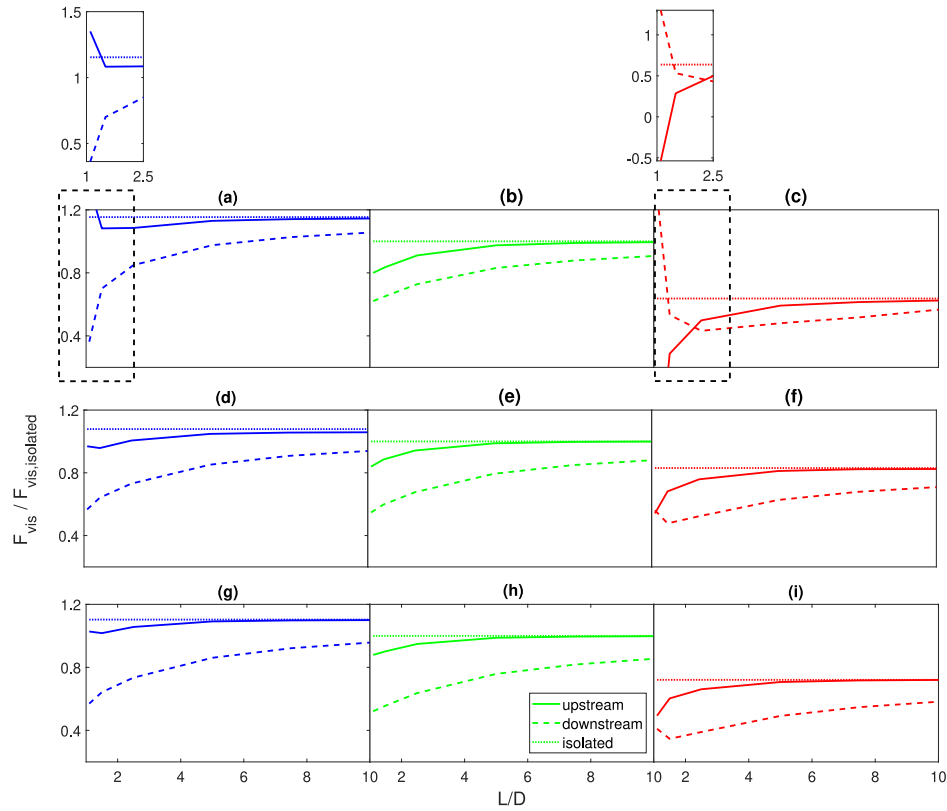
Fig. 11. Total viscous force, normalized with the value of an isolated particle without Stefan flow, as a function of the distance between particles (L/D). (a-c) $Re = 2.3$; (d-f) $Re = 7$; (g-i) $Re = 14$. (a,d, (g) $U_{Sf} = -0.2$ m s^{-1}; (b,e, (h) $U_{Sf} = 0$ m s^{-1}; (c,f, (i) $U_{Sf} = 0.6$ m s^{-1}.
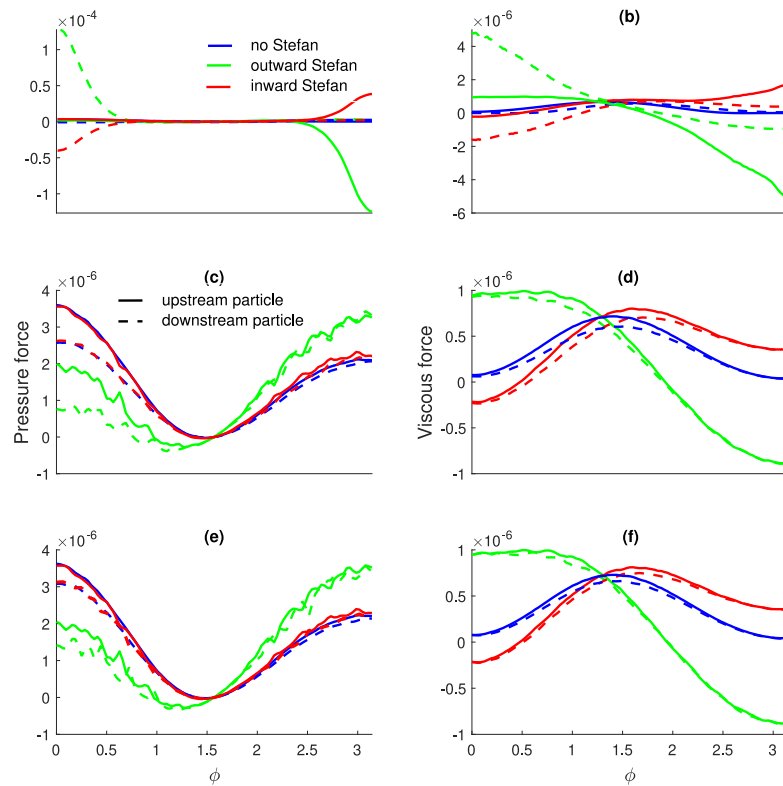

Fig. 12. Pressure force components (a,c,e) and viscous force components (b,d,f) of a slice going through the center of the particle in the flow direction ($Re = 2.3$) as a function of angle (ϕ) at the particle surface. Angle 0 corresponds to the front of each particle. (a, (b) $L/D = 1.1$; (c, (d) $L/D = 5$; (e, (f) $L/D = 10$. Solid lines: *upstream* particles; and dashed lines: *downstream* particle. Blue lines: without Stefan flow; green lines: outward Stefan flow; and red lines: inward Stefan flow. (For interpretation of the references to color in this figure legend, the reader is referred to the web version of this article.)
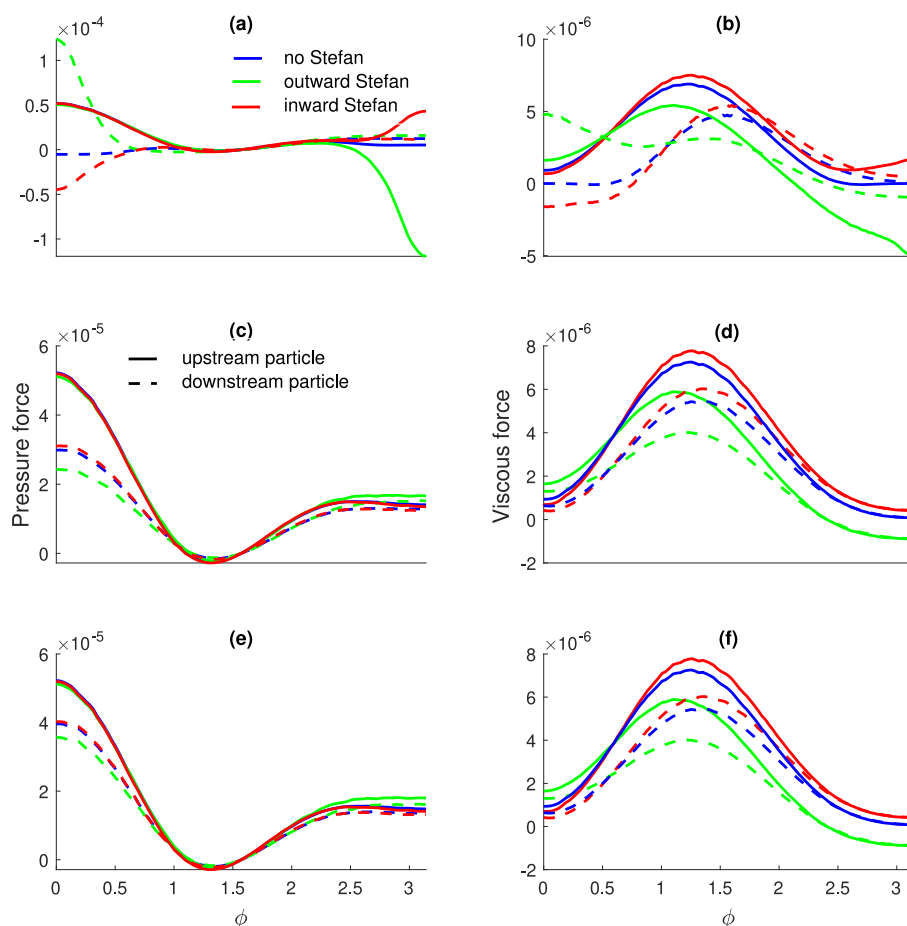
Fig. 13. Pressure force components (a,c,e) and viscous force components (b,d,f) of a slice going through the center of the particle in the flow direction ($Re = 14$) as a function of angle (ϕ) at the particle surface. Angle 0 corresponds to the front of each particle. (a, b) $L/D = 1.1$; (c, d) $L/D = 5$; (e, f) $L/D = 10$. Solid lines: *upstream* particles; and dashed lines: *downstream* particle. Blue lines: without Stefan flow; green lines: outward Stefan flow; and red lines: inward Stefan flow. (For interpretation of the references to color in this figure legend, the reader is referred to the web version of this article.)

particle. At these distances, the main role of an outward Stefan flow is to create high pressure and viscous forces between the particles. An outward Stefan flow creates very high pressure in the region between closely spaced particles, which results in a repulsive force between the two particles. In contrast, an inward Stefan flow produces an attractive force between the particles.

A model was developed for the drag coefficient of upstream and downstream particles with uniform Stefan flow around the particles. The model proposed here consists of three factors that describe different physical effects observed in the current and previous studies. A new model was developed to describe the interactions of two particles due to Stefan flow while previously developed models were adopted for individual effects of Stefan flow on an isolated particle and of neighboring particles. The model shows a good agreement with simulation data.

CRediT authorship contribution statement

Thamali R. Jayawickrama: Conceptualization, Methodology, Software, Validation, Formal analysis, Writing – original draft, Visualization. **M.A. Chishty:** Conceptualization, Writing – review & editing, Supervision. **Nils Erland L. Haugen:** Conceptualization, Writing – review & editing, Supervision, Funding acquisition. **Matthaus U. Babler:** Writing – review & editing, Supervision, Funding acquisition. **Kentaro Umeki:** Conceptualization, Methodology, Resources, Writing – review & editing, Supervision, Project administration, Funding acquisition.

Declaration of competing interest

The authors declare the following financial interests/personal relationships which may be considered as potential competing interests: Kentaro Umeki reports financial support and equipment, drugs, or supplies were provided by Swedish National infrastructure for Computing. Kentaro Umeki reports equipment, drugs, or supplies was provided by High Performance Computing Center North. Nils E. L. Haugen reports equipment, drugs, or supplies was provided by Norwegian research infrastructure services.

Data availability

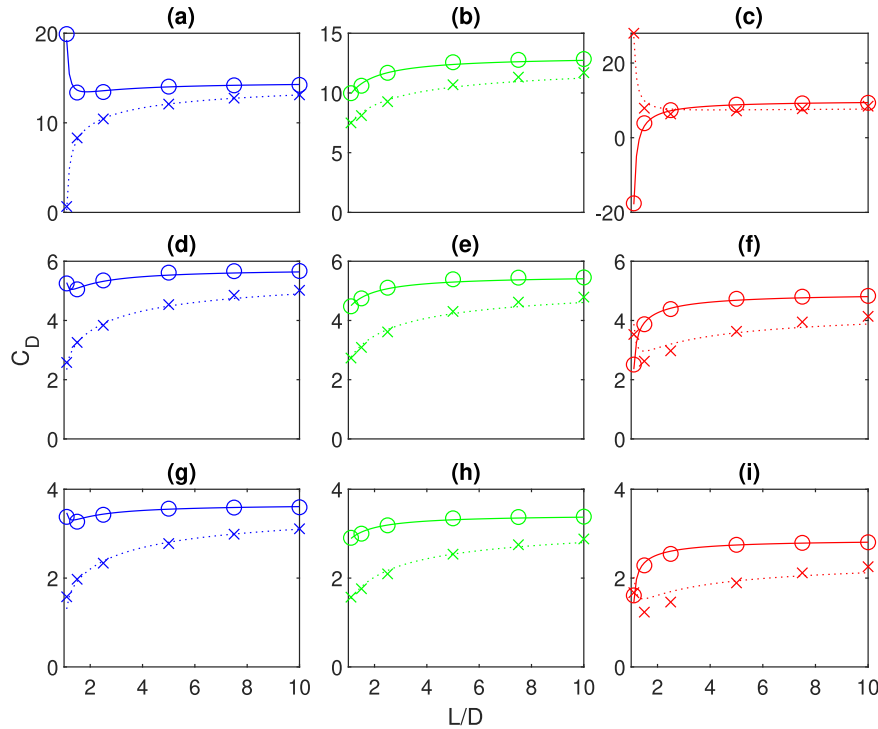Data will be made available on request

Fig. 14. Comparison of drag coefficient from the simulation and the model as a function of the distance between particles (L/D). (a-c) Re = 2.3; (d-f) Re = 7; (g-i) Re = 14. (a,d, (g) $U_{Sf} = -0.2$ m s^{-1}; (b,e, (h) $U_{Sf} = 0$ m s^{-1}; (c,f, (i) $U_{Sf} = 0.6$ m s^{-1}. ∘: upstream particle simulation data; ×: downstream particle simulation data; —: upstream particle model; ⋯: downstream particle model.

Appendix. Domain size and mesh refinement tests

In our previous work (Jayawickrama et al., 2019), we carried out simulations for an isolated spherical particle with a uniform Stefan flow immersed in a uniform, isothermal bulk fluid. The difference between our previous work and this work is the existence of one more particle in the streamwise direction. We used the same mesh refinement and the same mesh refinement region sizes of the previous work, although the domain size should vary. Therefore, we tested different domain sizes by varying both streamwise direction and transverse direction lengths. First, we added the length between the two particles (L/D) to the domain used in Jayawickrama et al. (2019) and kept the same transverse length (domain 1 in Table A.4). Two more domains were also tested, as shown in Table A.4. Domain test simulations were carried out for the lowest Reynolds number (Re=2.3), and highest outward Stefan flow case ($U_{Sf} = 0.6$), which generates the largest boundary layer around a particle based on our previous results (Jayawickrama et al., 2019, 2021). Drag coefficients obtained with the different domains were compared with the corresponding results from the largest domain (domain 2). Although domain 1 is smaller and still showed relatively small errors for drag coefficients, based on the velocity profiles around the two particles, domain 3 was selected for the simulations in this work. Drag coefficient results of different domains are shown in Table A.5.

Table A.4
Domain test details where $L = 10$, Re = 2.3 and $U_{Sf} = 0.624$. All the distances are in units of the particle diameter (D).

Domain	$D_{-x,1}$	$D_{+x,1}$	$D_{y,1}, D_{z,1}$
1	16	48	16
2	35	75	40
3	16	48	32

Table A.5
Domain size test for $Re = 2.3$, $L/D = 10$ and $U_{Sf} = 0.6$ with mesh refinement 0.02D at different domain sizes.

Domain	$C_{D,front}$	$C_{D,back}$	Error(% of domain 2)	
1	9.36	8.25	0.8	1.9
2	9.28	8.41	–	–
3	9.35	8.44	0.75	0.36

The refinement of the mesh closest to the particle in the single particle simulations was 0.01D, which was too expensive for the bigger domain with two particles. Simulations were also carried out for the smallest possible boundary layer i.e: where the Reynolds number is highest and the Stefan flow is inward. Results of the mesh refinement tests are shown in Table A.6. It is crucial to check whether this refinement (number of mesh between the two particles) is sufficient for $L/D = 1.1$. Therefore, the drag coefficient was compared for $L/D = 1.1$ and Re = 2.3, combined with either outward or no Stefan flow conditions, when the highest refinement is $0.01D$ and $0.02D$ (See Table A.7).

Table A.6

Mesh refinement test for $Re = 14$, $L/D = 2.5$ and $U_{Sf} = -0.2$.

Refinement	0.04D		0.02D		0.01D		0.005-Richardson extrapolation	
particle	front	back	front	back	front	back	front	back
C_d	3.32	2.95	3.43	2.34	3.47	2.37	3.48	2.38
Error(% of 0.005D)	4.34	24.75	1.18	1.30	0.3	0.3	0	0

Table A.7

Mesh refinement test for $Re = 2.3$, $L/D = 1.1$ and $U_{Sf} = -0.6$ and $U_{Sf} = 0$.

Refinement	0.02D		0.01D	
particle	front	back	front	back
$U_{Sf} = 0$				
C_d	9.98	7.49	10.13	7.58
Error(% of 0.01D)	1.48	1.19	0	0
$U_{Sf} = -0.623$				
C_d	−17.58	27.97	−17.67	28.81
Error(% of 0.01D)	0.51	2.92	0	0

References

Annamalai, K., Ryan, W., 1992. Interactive processes in gasification and combustion. Part I: Liquid drop arrays and clouds. Prog. Energy Combust. Sci. 18 (3), 221–295.

Chen, X., Du, S., Zhao, L., Yang, B., Zhou, Q., 2021. Effect of Stefan flow on the drag force in flow past random arrays of spheres. Chem. Eng. J. 412, http://dx.doi.org/10.1016/j.cej.2021.128691.

Chiang, C.H., Sirignano, W.A., 1993. Interacting, convecting, vaporizing fuel droplets with variable properties. Int. J. Heat Mass Transfer 36 (4), 875–886. http://dx.doi.org/10.1016/S0017-9310(05)80271-6.

Du, S., Zhao, L., Chen, X., Yang, B., Zhou, Q., 2022. Effect of Stefan flow on the drag force of single reactive particle surrounded by a sea of inert particles. Chem. Eng. Sci. 117546. http://dx.doi.org/10.1016/J.CES.2022.117546.

Dwyer, H.A., Stapf, P., Maly, R., 2000. Unsteady vaporization and ignition of a three-dimensional droplet array. Combust. Flame 121 (1–2), 181–194. http://dx.doi.org/10.1016/S0010-2180(99)00138-8.

García Llamas, Á.D., Guo, N., Li, T., Gebart, R., Løvås, T., Umeki, K., 2020. Morphology and volume fraction of biomass particles in a jet flow during devolatilization. Fuel 278, 118241. http://dx.doi.org/10.1016/J.FUEL.2020.118241.

Göktepe, B., Saber, A.H., Gebart, R., Lundström, T.S., 2016a. Cold flow experiments in an entrained flow gasification reactor with a swirl-stabilized pulverized biofuel burner. Int. J. Multiph. Flow. 85, 267–277. http://dx.doi.org/10.1016/j.ijmultiphaseflow.2016.06.016.

Göktepe, B., Umeki, K., Gebart, R., 2016b. Does distance among biomass particles affect soot formation in an entrained flow gasification process? Fuel Process. Technol. 141, 99–105. http://dx.doi.org/10.1016/j.fuproc.2015.06.038.

Haider, A., Levenspiel, O., 1989. Drag coefficient and terminal velocity of spherical and nonspherical particles. Powder Technol. 58, 63–70. http://dx.doi.org/10.1016/0032-5910(89)80008-7.

Jayawickrama, T.R., Haugen, N.E.L., Babler, M.U., Chishty, M., Umeki, K., 2019. The effect of Stefan flow on the drag coefficient of spherical particles in a gas flow. Int. J. Multiph. Flow. 117, 130–137. http://dx.doi.org/10.1016/j.ijmultiphaseflow.2019.04.022.

Jayawickrama, T.R., Haugen, N.E.L., Babler, M.U., Chishty, M.A., Umeki, K., 2021. The effect of Stefan flow on Nusselt number and drag coefficient of spherical particles in non-isothermal gas flow. Int. J. Multiph. Flow. 140, 103650. http://dx.doi.org/10.1016/j.ijmultiphaseflow.2021.103650.

Johnson, T.A., Patel, V.C., 1999. Flow past a sphere up to a Reynolds number of 300. J. Fluid Mech. 378, 19–70. http://dx.doi.org/10.1017/S0022112098003206.

Kékesi, T., Altimira, M., Amberg, G., Wittberg, L.P., 2019. International Journal of Multiphase Flow Interaction between two deforming liquid drops in tandem and various off-axis arrangements subject to uniform flow. Int. J. Multiph. Flow. 112, 193–218. http://dx.doi.org/10.1016/j.ijmultiphaseflow.2018.11.009.

Kim, I., Elghobashi, S., Sirignano, W.A., 1993. Three-dimensional flow over two spheres placed side by side. J. Fluid Mech. 246 (-1), 465–488. http://dx.doi.org/10.1017/S0022112093000229.

Kreitzberg, T., Pielsticker, S., Gvert, B.M., Kneer, R., 2016. CO2 and H2O Gasification under chemically and diffusion controlled conditions. In: 33rd Annual International Pittsburgh Coal Conference. Cape Town.

Llamas, Á.D.G., Guo, N., Li, T., Gebart, R., Umeki, K., 2022. Rapid change of particle velocity due to volatile gas release during biomass devolatilization. Combust. Flame 238, 111898. http://dx.doi.org/10.1016/j.combustflame.2021.111898.

Prahl, L., Hölzer, A., Arlov, D., Revstedt, J., Sommerfeld, M., Fuchs, L., 2007. On the interaction between two fixed spherical particles. Int. J. Multiph. Flow. 33 (7), 707–725. http://dx.doi.org/10.1016/j.ijmultiphaseflow.2007.02.001.

Prahl, L., Jadoon, A., Revstedt, J., 2009. Interaction between two spheres placed in tandem arrangement in steady and pulsating flow. Int. J. Multiph. Flow. 35 (10), 963–969. http://dx.doi.org/10.1016/j.ijmultiphaseflow.2009.05.001.

Raju, M.S., Sirignano, W.A., 1990. Interaction between two vaporizing droplets in an intermediate Reynolds number flow. Phys. Fluids A 2 (10), 1780–1796. http://dx.doi.org/10.1063/1.857705.

Saber, A.H., Göktepe, B., Umeki, K., Lundström, T.S., Gebart, R., 2016. Active fuel particles dispersion by synthetic jet in an entrained flow gasifier of biomass: Cold flow. Powder Technol. 302, 275–282. http://dx.doi.org/10.1016/j.powtec.2016.08.071.

Sayadi, T., Farazi, S., Kang, S., Pitsch, H., 2017. Transient multiple particle simulations of char particle combustion. Fuel 199, 289–298. http://dx.doi.org/10.1016/j.fuel.2017.02.096.

Sirignano, W.A., 1993. Fluid Dynamics of Sprays—1992 Freeman Scholar Lecture. Tech. rep..

Smoluchowski, B., 1911. Inter. Acad. Polonaise Sci. Lett. 28 (IA).

Stefanitsis, D., Strotos, G., Nikolopoulos, N., Gavaises, M., 2019. Numerical investigation of the aerodynamic breakup of a parallel moving droplet cluster. Int. J. Multiph. Flow 121, 103123. http://dx.doi.org/10.1016/j.ijmultiphaseflow.2019.103123.

Stimson, M., Jeffery, G.B., 1926. The motion of two spheres in a viscous fluid. Proc. R. Soc. Lond. Ser. A Cont. Pap. Math. Phys. Character 111 (757), 110–116. http://dx.doi.org/10.1098/RSPA.1926.0053.

Sun, B., Tenneti, S., Subramaniam, S., 2015. Modeling average gas–solid heat transfer using particle-resolved direct numerical simulation. Int. J. Heat Mass Transfer 86, 898–913. http://dx.doi.org/10.1016/j.ijheatmasstransfer.2015.03.046.

Umeki, K., Kirtania, K., Chen, L., Bhattacharya, S., 2012. Fuel Particle Conversion of Pulverized Biomass during Pyrolysis in an Entrained Flow Reactor. Ind. Eng. Chem. Res. 51, 13973–13979. http://dx.doi.org/10.1021/ie301530j.

Wang, J., Huang, X., Qiao, X., Ju, D., Sun, C., 2020. Experimental study on evaporation characteristics of single and multiple fuel droplets. J. Energy Inst. 93 (4), 1473–1480. http://dx.doi.org/10.1016/j.joei.2020.01.009.

Wang, Y., Zhang, M., Wang, H., Jin, H., 2022. The influence of Stefan flow on the flow and heat-transfer characteristics of spherical-particle pair in supercritical water. Int. J. Multiph. Flow. 151, 104045. http://dx.doi.org/10.1016/j.ijmultiphaseflow.2022.104045.

Weller, H.G., Tabor, G., Jasak, H., Fureby, C., 1998. A tensorial approach to computational continuum mechanics using object-oriented techniques. Comput. Phys. 12 (6), 620. http://dx.doi.org/10.1063/1.168744.

Wu, G., Sirignano, W.A., 2011a. Combustion Theory and Modelling Transient convective burning of interactive fuel droplets in single-layer arrays. Combust. Theory Model. http://dx.doi.org/10.1080/13647830.2010.535567.

Wu, G., Sirignano, W.A., 2011b. Transient convective burning of interactive fuel droplets in double-layer arrays. Combust. Flame 158 (12), 2395–2407. http://dx.doi.org/10.1016/j.combustflame.2011.04.011.

Yali Tang, Y., Frank Peters, E.A., Hans Kuipers, J.A., Sebastian Kriebitzsch, S.H., Martin van der Hoef, M.A., 2015. A new drag correlation from fully resolved simulations of flow past monodisperse static arrays of spheres. AIChE J. 61 (2), 688–698. http://dx.doi.org/10.1002/AIC.14645.

Zhu, C., Liang, S.-c., Fan, L.-s., 1994. Particle wake effects on the drag force of an interactive particle. Int. J. Multiph. Flow. 20 (1).